Korean J. Chem. Eng., **25**(6), 1362-1371 (2008)

Development of a reactive puff model for simultaneous consideration of plume dispersion and plume chemistry

Hyun Soo Kim, Mee Kyung Lee, Hyun Jung Cho, and Chul Han Song†

Department of Environmental Science and Engineering, Gwangju Institute of Science and Technology (GIST), Gwangju 500-712, Korea

(*Received 17 October 2007 • accepted 2 June 2008*)

Abstract–To comprehensively assess and understand the environmental impacts of air pollutants emitted from large-scale point sources, the complex, non-linear photochemistry inside the plumes should be considered together with atmospheric turbulent dispersion of the air pollutants. For this purpose, a reactive puff model that can consider both atmospheric turbulent dispersion and photochemical reactions was developed in this study. The model's performance was evaluated by comparing the model-predicted concentrations with the ship-plume chemical concentrations measured from the Intercontinental Transport and Chemical Transformation (ITCT) 2K2 field campaign. This comparison study confirmed the ability of the developed reactive puff model to capture the major characteristics of both plume dispersion and photochemical reactions. Based on these findings, the reactive puff model was applied to a Korean power plant (Hadong) as a case study.

Key words: Reactive Puff Model, Gaussian Plume Dispersion, Atmospheric Photochemical Reaction, Environmental Impact Assessment (EIA), ITCT 2K2

INTRODUCTION

Air pollution is one of the major environmental problems in Korea as a consequence of its rapid industrialization and urban growth [e.g., 1]. To reduce the environmental impact of air pollutants, the Korean Ministry of Environment (KMoE) started to implement the Total Air Pollution Load Management System in 2007 for reducing the total emissions of "primary pollutants," such as NO_x and SO_2, particularly from the large-scale point sources. However, in terms of air toxicity, "secondary air pollutants" formed via atmospheric photochemistry of the primary pollutants, such as ozone, PANs (peroxyacetyl nitrates), aldehydes, and acidic substances, have more harmful effects on human health than the "primary pollutants" do. There are complex non-linear relationships between the primary pollutants and secondarily formed toxic pollutants in the atmosphere. For a comprehensive analysis of the environmental impacts of the primary pollutants, emitted from the large-scale point sources, the complex relationships between the primary and secondary pollutants should be considered. However, the plume and/or puff models currently being used to analyze the environmental impacts of the large point-source emissions only consider the impacts of the turbulent dispersion (e.g., Industrial Source Complex, ISC3), or can only account for the turbulent dispersion and atmospheric chemical transformations in a very simple manner (e.g., California Puff, CALPUFF v.5) [2,3].

In order to consider the production of secondary toxic pollutants from the primary air pollutants emitted from the large-scale point sources such as power-plants, petrochemical facilities, and smelting factories, the need for simultaneous consideration of turbulent eddy dispersion and atmospheric chemical transformation should be satisfied by integrating a turbulent dispersion scheme with a full "atmospheric chemical mechanism." In this study we therefore tried to combine a Gaussian plume dispersion scheme with atmospheric photochemical reactions. The strategy taken in this study is outlined here: (1) To consider the turbulent dispersion of the plume, we chose formulas suggested by Briggs [4] and Hanna et al. [5,6]. The formulas can simulate the transport of air pollutants based on a Gaussian plume dispersion. (2) For consideration of the plume chemistry, a modified version of Lurmann et al.'s [7] chemical mechanism was combined with the Gaussian turbulent plume dispersion scheme. (3) The performance of the developed reactive puff (plume) model was then evaluated by comparing the model-predicted plume concentrations with the plume chemical concentrations measured from the Intercontinental Transport and Chemical Transformation 2002 (ITCT 2K2) campaign. (4) After evaluating the model performance, we applied the reactive puff model to a power-plant case to show the capability of the developed reactive puff model, and also to test the reactive puff model as a tool for a more comprehensive environmental impact assessments (EIA) for the large-scale point source emissions.

DEVELOPMENT OF A REACTIVE PUFF MODEL

We combined a photochemical reaction mechanism with a turbulent puff dispersion scheme. The dynamic components of this study were based on Briggs [4] and Hanna et al.'s [5,6] parameterizations, and the chemical components were based on the modified version of Lurmann et al.'s [7] condensed chemical reactions.

1. Physical Component of Reactive Puff Model

The central concentration in the plume can be expressed as a func-

†To whom correspondence should be addressed.
E-mail: chsong@gist.ac.kr

‡This article is dedicated to Professor Chang Kyun Choi for celebrating his retirement from the School of Chemical and Biological Engineering, Seoul National University.

tion of standard deviation of vertical and lateral concentrations of distributions as shown below:

$$\frac{C}{Q}=\frac{1}{\pi u\sigma_y\sigma_z} \tag{1}$$

where Q is the mass emission rate (g/sec) from the point source, u is the wind speed, σ_y and σ_z and are the standard deviations of the lateral and vertical concentration distribution, respectively. The dispersion parameters of the standard deviations are calculated by the standard formulas listed below [5]:

$$\sigma_y=\sigma_v t f_y\left(\frac{t}{T_{Ly}}\right) \tag{2}$$

$$\sigma_z=\sigma_w t f_z\left(\frac{t}{T_{Lz}}\right) \tag{3}$$

where σ_v and σ_w are the standard deviations for the lateral and vertical fluctuation in the turbulent velocity, respectively, t is the travel time from the large-scale point source, f_y and f_z are universal dimensionless functions that equal unity at small t/T_L, and T_{Ly} and T_{Lz} are the lateral and vertical Lagrangian integral timescales for turbulence, respectively.

In order to calculate the lateral and vertical dispersion parameters, it is necessary to prescribe the variables σ_v, σ_w, T_{Ly}, and T_{Lz} in Eqs. (2) and (3). Fortunately, considerable research efforts have targeted this problem over several decades and a wealth of information is available. For example, Briggs's [4] and Hanna et al.'s [5,6] formulas for σ_y and σ_z over rural and ocean surfaces are listed and summarized in Tables 1 and 2, based on the downwind distances and stability classes.

Since the boundary layer is often capped by inversion at height h, called the mixing height, it is generally assumed that plumes will not be dispersed above the mixing height. At this point, σ_z is not allowed to increase beyond about 0.8 h [8]. Plumes are well mixed vertically, once they occupy most of the mixing height.

Table 1. Formulas for lateral and vertical dispersion coefficients, σ_y (x) and σ_z (x), as a function of downwind distance, x(m), for rural conditions over land[a]

Pasquill stability class	σ_y, m	σ_z, m
Downwind distance x(m) is less than 1 km		
A	$0.22x(1+0.0001x)^{-1/2}$	0.20x
B	$0.16x(1+0.0001x)^{-1/2}$	0.12x
C	$0.11x(1+0.0001x)^{-1/2}$	$0.08x(1+0.0002x)^{-1/2}$
D	$0.08x(1+0.0001x)^{-1/2}$	$0.06x(1+0.0015x)^{-1/2}$
E	$0.06x(1+0.0001x)^{-1/2}$	$0.03x(1+0.0003x)^{-1}$
F	$0.04x(1+0.0001x)^{-1/2}$	$0.01x(1+0.0003x)^{-1}$
Downwind distance x(m) is greater than 10 km		
A	0.156x	0.20x
B	0.113x	0.12x
C	0.078x	$0.08x(1+0.0002x)^{-1/2}$
D	0.057x	$0.06x(1+0.0015x)^{-1/2}$
E	0.042x	$0.03x(1+0.0003x)^{-1}$
F	0.028x	$0.01x(1+0.0003x)^{-1}$

[a]Briggs [4] and Hanna et al. [5]

Table 2. Formulas for lateral and vertical dispersion coefficients, σ_y(x) and σ_z(x), as a function of downwind distance, x(m), over the ocean

Pasquill stability class	σ_y, m	σ_z, m
Downwind distance x(m) is less than 10 km		
A	$0.11x(1+0.0001x)^{-1/2}$	0.10x
B	$0.08x(1+0.0001x)^{-1/2}$	0.06x
C	$0.055x(1+0.0001x)^{-1/2}$	$0.04x(1+0.0002x)^{-1/2}$
D	$0.04x(1+0.0001x)^{-1/2}$	$0.03x(1+0.0015x)^{-1/2}$
E	$0.03x(1+0.0001x)^{-1/2}$	$0.015x(1+0.0003x)^{-1}$
F	$0.02x(1+0.0001x)^{-1/2}$	$0.008x(1+0.0003x)^{-1}$
Downwind distance x(m) is greater than 10 km		
A	0.078x	0.10x
B	0.057x	0.06x
C	0.039x	$0.04x(1+0.0002x)^{-1/2}$
D	0.028x	$0.03x(1+0.0015x)^{-1/2}$
E	0.021x	$0.015x(1+0.0003x)^{-1}$
F	0.014x	$0.008x(1+0.0003x)^{-1}$

Based on the formulas presented, the concentration of species i at time steps k and k+1 ($C_{i,k}$ and $C_{i,k+1}$) can be calculated by:

$$C_{i,k}=\frac{Q_i}{\pi u(\sigma_y\sigma_z)_k} \tag{4}$$

$$C_{i,k+1}=\frac{Q_i}{\pi u(\sigma_y\sigma_z)_{k+1}} \tag{5}$$

where $(\sigma_y\sigma_z)_k$ and $(\sigma_y\sigma_z)_{k+1}$ represent the products of σ_y and σ_z at time steps k and k+1, respectively. Both Q_i and u are assumed to be constant during the period being considered. The dilution factor at time step k ($Dil_{i,k}$), is estimated from the ratio of the products of the lateral and vertical dispersion coefficient for time steps k and k+1:

$$Dil_{i,k}=\frac{C_{i,k+1}}{C_{i,k}}=\frac{(\sigma_y\sigma_z)_k}{(\sigma_y\sigma_z)_{k+1}} \tag{6}$$

Likewise, the dilution factor expression for the case where σ_z is larger than 0.8 h, under the assumption of constant mixing height, is as follows:

$$Dil_{i,k}=\frac{C_{i,k+1}}{C_{i,k}}=\frac{(\sigma_y)_k}{(\sigma_y)_{k+1}} \tag{7}$$

These dilution factors can be expressed as the ratio of plume cross

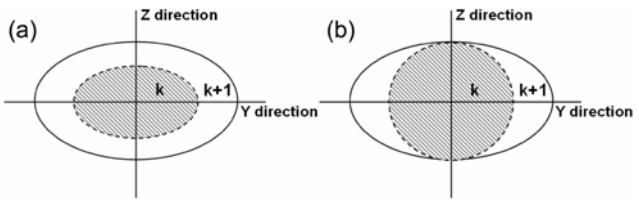

Fig. 1. Illustration of an elliptical puff dispersion: (a) σ_z<0.8 h and (b) σ_z≥0.8 h.

sectional area at time step k to that at time step k+1. During the dispersion, the plume is dispersed elliptically, as shown in Fig. 1. When σ_z is less than 0.8 h, the plume develops both horizontally and vertically, as illustrated in panel (a) of Fig. 1. However, when the vertical dispersion factor is larger than 0.8 h, which means the fully dispersed plume reaches mixing height, no more dispersion occurs vertically, and only the lateral dispersion is important, as depicted in panel (b) in Fig. 1.

The concentration of a certain species i, can be expressed by Eq. (8) by using the dilution factor [9,10]:

$$C_{i,k+1}=Dil_k C_{i,k}+(1-Dil_k)C_{i,b} \quad (8)$$

Table 3. Several chemical reactions used in the reactive puff model

	Reactions	Rate Constant k (cm^3 $molecule^{-1}$ s^{-1} units)
[R1]	$NO_2+hv\rightarrow NO+O_3$	J_1
[R2]	$NO+O_3\rightarrow NO_2+O_2$	$2.2\times10^{-12}e^{-1430/T}$
[R3]	$NO_2+O_3\rightarrow NO_3+O_2$	$1.2\times10^{-13}e^{-2450/T}$
[R4]	$NO+NO_3\rightarrow 2NO_2$	$1.7\times10^{-11}e^{150/T}$
[R5]	$NO_2+NO_3\xrightarrow{+M}N_2O_5$	1)
[R6]	$N_2O_5\rightarrow NO_2+NO_3$	2)$k_5 7.5\times10^{26}(300/T)^{0.32}e^{-11080/T}$
[R7]	$NO_2+NO_3\rightarrow NO+NO_2+O_2$	$2.50\times10^{-14}e^{-1230/T}$
[R8]	$NO_3+hv\rightarrow 0.15NO+0.85NO_2+0.85O_3+O_2$	$3.29J_1$
[R9]	$NO_3+HO_2\rightarrow HNO_3+O_2$	2.5×10^{-12}
[R10]	$O_3+hv\rightarrow 2OH$ (H_2O dependent)	3)$k_{10a}7.6\times10^{-6}[H_2O]$
[R11]	$NO+OH\xrightarrow{+M}HO+NO$	1)
[R12]	$HONO+hv\rightarrow NO+OH$	$0.205J_1$
[R13]	$NO_2+OH\xrightarrow{+M}HNO_3$	1)
[R14]	$HNO_3+hv\rightarrow NO_2+OH$	J_{14}
[R15]	$HNO_3+OH\rightarrow NO_3+H_2O$	$9.4\times10^{-15}e^{778/T}$
[R16]	$N_2O_5+H_2O\rightarrow 2HNO_3$	1.30×10^{-21}
[R17]	$CO+OH\rightarrow HO_2+CO_2$	$1.5\times10^{-13}(1+1.04\times10^{-22}T[M])/(1+2.6\times10^{-23}T[M])$
[R18]	$O_3+OH\rightarrow HO_2+O_2$	$1.6\times10^{-12}e^{-1000/T}$
[R19]	$NO+HO_2\rightarrow NO_2+OH$	$3.7\times10^{-12}e^{240/T}$
[R20]	$NO_2+HO_2\rightarrow HNO_4$	$6.9\times10^{-33}e^{1007/T}[M]/[1+4.86\times10^{-12}([M]^{0.61})]$
[R21]	$HNO_4\rightarrow NO_2+HO_2$	$4.9\times10^{-6}e^{-10015/T}[M]/[1+4.86\times10^{-12}([M]^{0.61})]$
[R22]	$O_3+HO_2\rightarrow OH+2O_2$	$1.4\times10^{-14}e^{-600/T}$
[R23]	$HO_2+HO_2\rightarrow H_2O_2+O_2$ (H_2O dependent)	$[2.2\times10^{-13}e^{620}/T+1.9\times10^{-33}[M]e^{980/T}]\times[1+1.4\times10^{-27}[M][H_2O]e^{2200/T}]$
[R24]	$H_2O_2+hv\rightarrow 2OH$	J_{24}
[R25]	$H_2O_2+OH\rightarrow HO_2+H_2O$	$3.3\times10^{-12}e^{-200/T}$
[R26]	$NO_2+H_2O\rightarrow HONO+HNO_3$-$NO_2$	4.00×10^{-24}
[R27]	$HNO_4+hv\rightarrow NO_2+HO_2$	$1.0\times10^{-4}J_1$
[R28]	$HNO_4+OH\rightarrow NO_2+H_2O+O_2$	$1.3\times10^{-12}e^{380/T}$
[R29]	$SO_2+OH\xrightarrow{+M}SO_4+HO_2$	1)
[R30]	$HCHO+hv\rightarrow 2HO_2+CO$	J_{30}
[R31]	$HCHO+hv\rightarrow CO+H_2$	J_{31}
[R32]	$HCHO+OH\rightarrow HO_2+CO+H_2O$	1.00×10^{-11}
[R33]	$HCHO+HO_2\rightarrow AHO_2$	1.00×10^{-14}
[R34]	$AHO_2+NO\rightarrow ACO_2+HO_2+NO_2$	$4.2\times10^{-12}e^{180/T}$
[R35]	$AHO_2+HO_2\rightarrow ACO_2+H_2O+O_2$	2.00×10^{-12}
[R36]	$2AHO_2\rightarrow ACO_2+2HO_2+2O_2$	1.00×10^{-13}
[R37]	$ACO_2+OH\rightarrow HO_2+H_2O+CO_2$	3.20×10^{-13}
[R38]	$NO_3+HCHO\rightarrow HNO_3+HO_2+CO$	6.00×10^{-16}

1) $\left[\frac{k_0(T)^{m_0}[M]}{1+\{k_0(T)^{m_0}[M]/k_\infty(T)^{m_\infty}\}}\right]F^{[1+(log_{10}(k_0(T)^{m_0}[M]/k_\infty(T)^{m_\infty}))^2]^{-1}}$ [7] ([H_2O] is water vapor concentration, ppm; T is temperature, K; [M] is Number density of air, molecules cm^{-3})

2) k_5 rate constant for $NO_2+NO_3\rightarrow N_2O_5$ [18]

3) k_{10a} photolytic rate of $O_3+hv\rightarrow O(^1D)$

4) Based on the environmental chamber experimental data [19]

where $C_{i,b}$ is the background concentration of species i. If we assume that $C_{i,b}$ is 0, then Eq. (8) can be further simplified into Eqs. (6) and (7). By using this relation, the concentration change in species i due to dilution (ΔC_i^D) can be expressed as:

$$\Delta C_i^D = C_{i,k+1} - C_{i,k} = (Dil_k - 1)C_{i,k} + (1 - Dil_k)C_{i,b} \quad (9)$$

The concentration change in species i due to gas-phase chemistry can be expressed as:

$$\Delta C_i^R = [F_{i,k}(C_1 \ldots C_n) - Des_{i,k}(C_1 \ldots C_n)C_{i,k}]\Delta t \quad (10)$$

where $F_{i,k}(C_1 \ldots C_n)$ represents the formation rate of species i due to chemical reactions, and $Des_{i,k}(C_1 \ldots C_n)C_{i,k}$ indicates the destruction rate. The net change in concentration for species i can, therefore, be estimated from the sum of changes due to dilution and chemical reaction as:

$$\Delta C_i^N = \Delta C_i^D + \Delta C_i^R \quad (11)$$

2. Chemical Component of Reactive Puff Model

The developed puff model includes Lurmann et al.'s [7] condensed mechanism which consists of 71 O_3-H_xO_y-N_xO_y-CH_4 related reactions and 184 NMHC (non-methane hydrocarbons) reactions, but with some major modifications. These include appropriately updated rate coefficients and additional NO_x and organic peroxide reactions [e.g., 11-13]. The 38 chemical reactions related to O_3-H_xO_y-N_xO_y-CH_4 reactions are shown in Table 3. The photolysis rate coefficients used in this study were those based on a DISORT 4-stream implementation of the NCAR TUV radiative code with an updated $O(^1D)$ quantum yield [14]. In addition, several gas/aqueous-phase sulfur reactions/equilibria processes were also included for studying the chemical evolution and fate of sulfur species in the atmosphere [8]. Several sulfur-involved heterogeneous processes were also incorporated for gas-aerosol reactions.

The solutions of the ordinary differential equations that describe the time-dependent variations in atmospheric species concentrations were achieved by using the Gear Ordinary Differential Equation (ODE) solver. Because of the nature of the Gear solver, which is an implicit solver recently improved for atmospheric chemistry studies, the time intervals for integrating the ordinary differential equations were automatically controlled from a few seconds to several minutes.

Geographical, meteorological, and photochemical information was fed into the Lagrangian model and each run was executed until quasi steady-state conditions were reached for all time varying species. At this point, an instantaneous "puff" of NO_x and SO_2 was injected into the system, thereby initializing what will be labeled hereafter as "plume chemistry". In the evolution of this plume chemistry, the effect of the initial NO_x perturbation was examined in terms of the changing concentration levels of $O_3/NO_x/HO_x$, as well as of other oxidant products. These were tracked in time until most species approached their background levels.

EVALUATION OF REACTIVE PUFF MODEL

As afore mentioned, the concentrations of puff can be expressed as a function of standard deviation of the vertical and lateral concentrations of distribution. The dispersion parameter can be expressed as a function of downwind distance and stability class, based on the dispersion region. To evaluate the performance of the developed reactive puff model, a comparison study between the observations and predictions was made.

Due to the lack of the plume measurement data in Korea, ship-plume chemical concentrations measured during the NOAA ITCT 2K2 campaign over the Northeast Pacific Ocean were used for the comparison study. The comparison study between the model-predicted and measured plume concentrations over the "remote ocean surfaces" introduces a further advantage: since the plume disperses long distances over the flat and homogeneous ocean surfaces, the

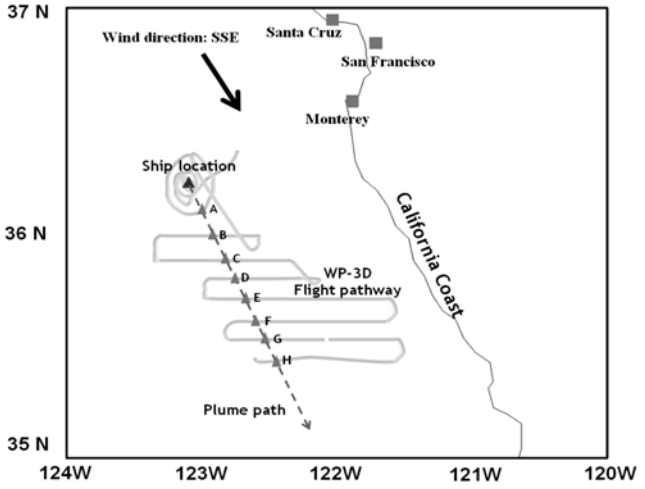

Fig. 2. ITCT 2K2 ship plume sampling, showing both plume path and WP-3D flight track.

Table 4. Simulation conditions used in this study

Variables	Values
Emission rates	
NO_x (g/s)	6.25
SO_2 (g/s)	9.38
Meteorological conditions	
Stability class[a]	Neutral, Stable
Wind velocity (m/s)	10
Wind direction	SSE
Location of ship	
Latitude (°N)	36.19
Longitude (°W)	123.06
Aerosol-related variables	
Aerosol surface area ($\mu m^2/cm^3$)	90
pH[b]	6.9
Background concentrations (ppbv)	
$[NO_x]$	0.15
$[O_3]$	40
[CO]	130
$[SO_2]$	0.16
$[C_3H_8]$	0.37

[a]Only two stability classes were considered (refer to text)
[b]Assumed [8]

uncertainties resulting from the complex geographical structures and frequently varying meteorological conditions over a land-based comparison could be excluded. During the ITCT 2K2 field campaign, the WP-3D aircraft measured gas-phase species, particulate pollutants concentrations, and metrological parameters. As shown in the track of the WP-3D aircraft, the gas and particulate pollutants were measured at eight locations from A to H (Fig. 2). The initial conditions and background conditions were also measured and are summarized in Table 4. The chemical tracer and wind pattern observations suggested that this region was moderately polluted. The median background levels of NO_x, O_3, SO_2 and CO around the ship plumes were 150 pptv, 40 ppbv, 160 pptv, and 130 ppbv, respectively. The levels of several NMHC species were also observed. For example, the median C_3H_8 concentration was 370 pptv. The wind direction was SSE at wind speeds of 4-11 (m/sec). The ship speed was about 5 (m/sec). By considering the wind direction and the ship and wind velocities, the calculated net velocity ranged from approximately 7.0 to 14.0 (m/sec). In order to consider the entire range of net resultant wind velocities, simulations were performed from 7 to 14 m/sec. Stability classes were assumed as neutral (D) and stable (F), because the most frequent stability classes over the remote surfaces ocean are between neutral and stable, based on Frick and Hopel's [15] experimental study. Frick and Hopel tried to experimentally determine the most frequent stability classes in the marine boundary layer (MBL), as a part of the Monterey Area Ship Track (MAST) Experiment. This experiment was actually performed over almost the same locations of the plume measurements by WP-3D aircraft. The results of their study indicated that the most frequent stability classes were between neutral (D) and stable (F). The emission rates of NO_x and SO_2 from the ship were also reported at 6.25 (g/sec) and 9.38 (g/sec), respectively. Considering the conditions, four cases were assumed to describe the likely conditions of the ship plume development (Table 5).

Figs. 3 and 4 show the comparison results at the three transects of the plume (locations of A, C, and H). The x and y axes represent the lateral distances from the centerline of the plume and concentrations of NO_x and SO_2, respectively. The puff aging times of the three transects were 39.8, 80.0, and 176.0 (min) at the locations A, C, and H, respectively. From the three transects, the concentrations of NO_x and SO_2 emitted from the ship were decreased, which may indicate that turbulent dispersion and chemical loss process caused the concentration decreases (Note that the scale of the y-axises were kept the same for the comparison purpose in Figs. 3 and 4).

In addition, the comparisons of the observed and predicted O_3 concentrations are presented in Fig. 5(a). When the ship emits a puff, ozone is almost instantaneously titrated by NO (refer to [R1]), since 95% of the NO_x emitted from the ship is occupied by NO:

Table 5. Conditions applied to the reactive plume model in the comparison study

Case	Wind velocity (m/s)	Stability class
I	14	D
II	14	F
III	7	D
IV	7	F

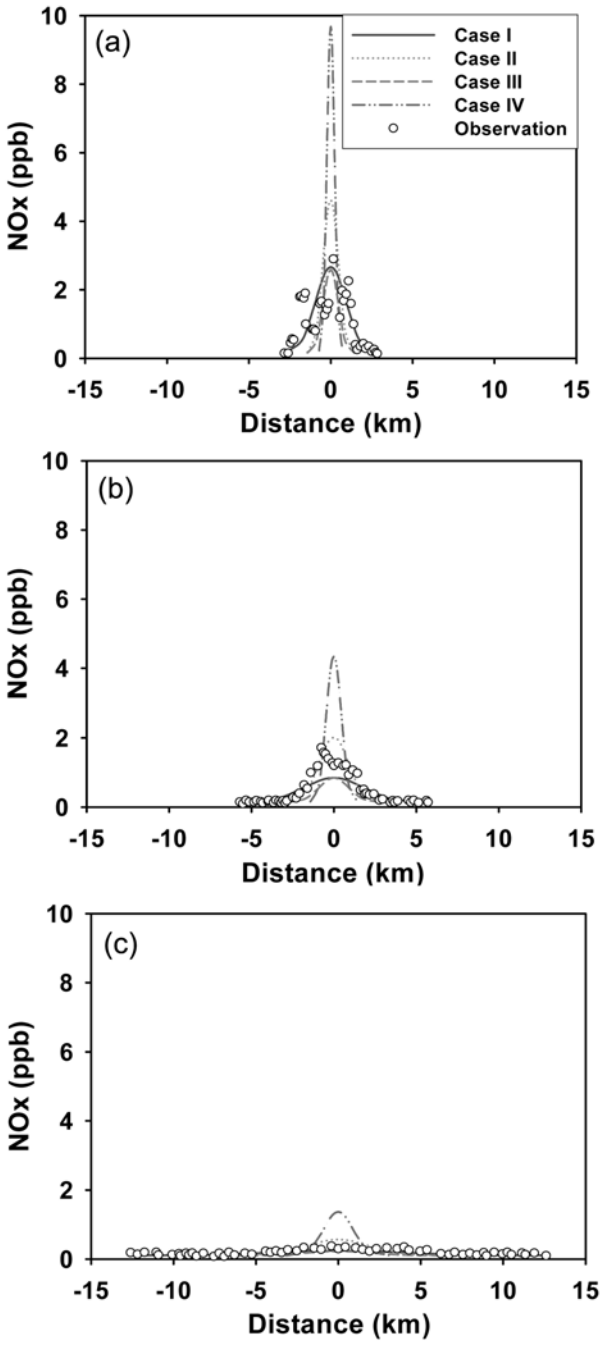

Fig. 3. Comparisons between predicted and observed NO_x concentrations at locations: (a) A, (b) C, and (c) H.

$$NO+O_3 \rightarrow NO_2+O_2 \quad [R1]$$

As mentioned previously, the background ozone concentration was 40 ppbv, and because of the ozone titration very near the ship stack, the ozone concentration dropped to nearly 0 ppbv and then slowly recovered as the NO_2 (temporary storage of ozone) was photo-dissociated and converted back to O_3:

$$NO_2+h\nu \rightarrow NO+O^{3P} \quad [R2]$$

$$O^{3P}+O_2 \rightarrow O_3 \quad [R3]$$

This ozone recovery is apparently shown in Fig. 5(a), as evidenced

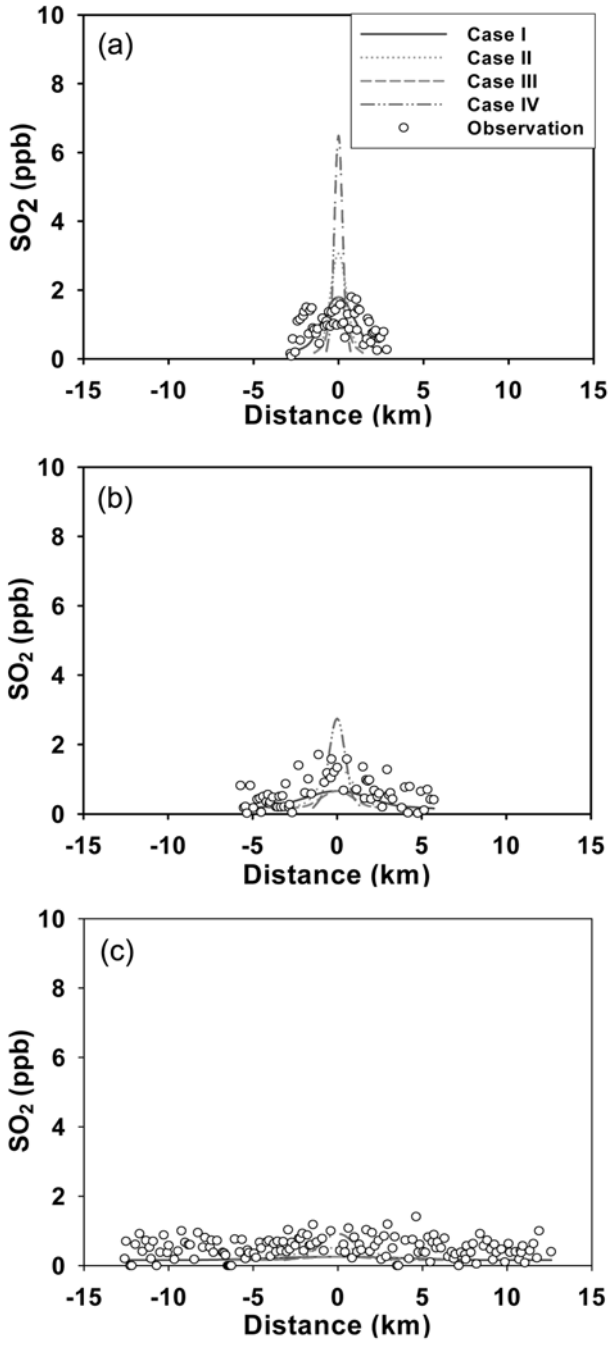

Fig. 4. Comparisons between predicted and observed SO_2 concentrations at locations: (a) A, (b) C, and (c) H.

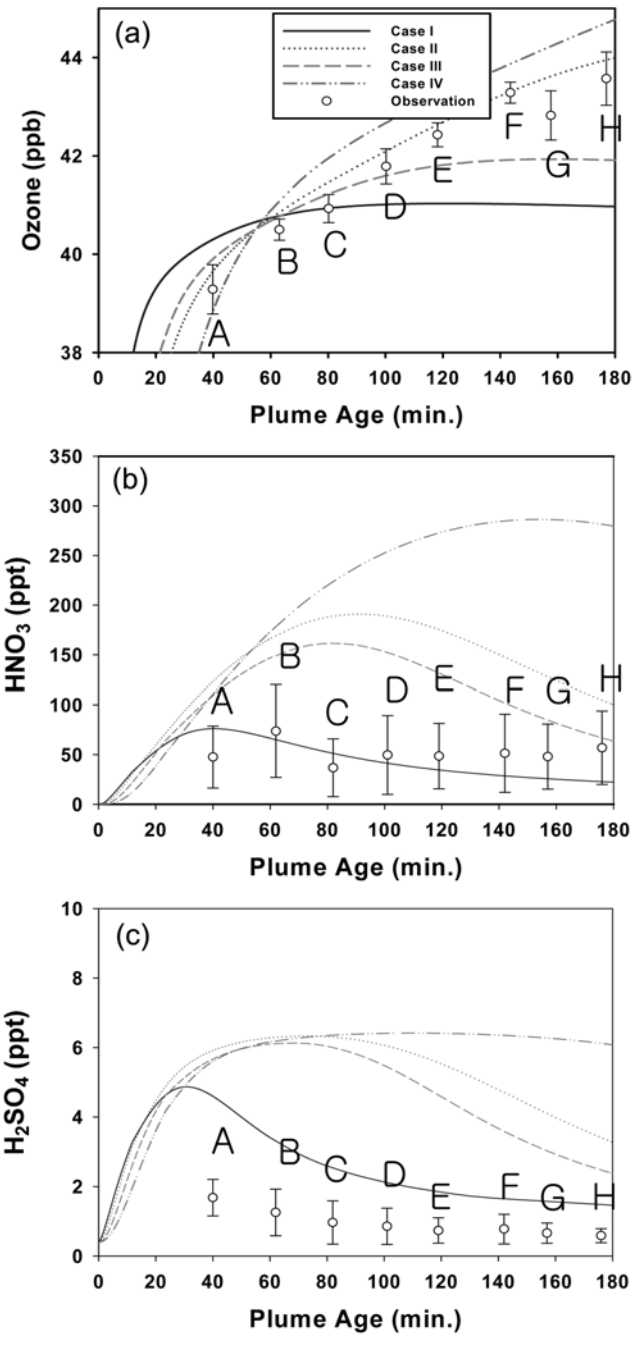

Fig. 5. Comparisons between predicted center-line and observed three gas phase pollutant concentrations at eight observation points: (a) O_3, (b) HNO_3, and (c) H_2SO_4.

by inspection of the ozone concentrations between 0 and 40 minutes, which is often called the "ozone recovery zone". At the end of the ozone recovery zone, the ozone concentration reached the background concentration of 40 ppbv. The ozone recovery time depended on the stability class, wind speed, and NO_x emission rates. In general, the predicted primary and secondary pollutant concentrations agreed well with the observations.

Further comparisons were made for the two acidic, gas-phase species: nitric acid (HNO_3) and sulfuric acid (H_2SO_4). Both HNO_3 and H_2SO_4 are produced via the oxidation with hydroxyl radicals (OH) in the atmosphere:

$$NO_2 + OH \xrightarrow{M} HNO_3 \quad [R4]$$

$$SO_2 + OH \xrightarrow[multi\ step]{M} H_2SO_4 \quad [R5]$$

Shown in Figs. 5(b) and 5(c) are the variations of the HNO_3 and H_2SO_4 concentrations with respect to the puff travel times. In the productions of both HNO_3 and H_2SO_4, the OH radical concentration is important (refer to [R4] and [R5]). The OH radicals are typically produced via [R6] and [R7] in the MBL:

$$O_3 + h\nu \rightarrow O^{1D} + O_2 \quad [R6]$$

$O^{1D}+H_2O \rightarrow 2OH$ [R7]

As indicated by [R6], the OH radical formation is initiated by the photodissociation of O_3. As discussed previously, O_3 is titrated near the ship stack. Therefore, OH also initially disappears near the ship stack, and then gradually gets back. Accordingly, both HNO_3 and H_2SO_4 concentrations disappear near the ship stack, and then gradually increase back. The reactive puff model (particularly, case I) can reasonably well match the observed HNO_3 concentrations (Fig. 5(b)). However, our model tends to over-predict the H_2SO_4 concentrations (Fig. 5(c)). In actuality, it is difficult to accurately predict the two acidic species concentrations in the atmosphere, since there exist many uncertainties and unknown atmospheric processes (e.g., uncertain heterogeneous rates of nitrate and sulfate formation from gas-phase HNO_3 and H_2SO_4).

Table 6. Variables applied to the Hadong power-plant simulations

Variables	Values	
	Over the rural	Over the ocean
Meteorological conditions		
Stability class		Neutral (D)
Wind speed (m/s)		5
Average mixing height (m)		700
Location		
Latitude (°N)		34.98
Longitude (°E)		128.83
Emission rates		
NO_x (g/s)		47.61
SO_2 (g/s)		30.00
Aerosol-related variables		
Background aerosol type	Rural	Marine
Aerosol surface area ($\mu m^2/cm^3$)[a]	139	43.3
α_{N2O5}	0.1	0.1
α_{NO3}	0.01	0.01
α_{SO2}	0.01	0.01
D_{SO2}	0.103	0.103
α_{H2SO4}	0.5	0.5
D_{H2SO4}	0.088	0.088
pH[b]	4.5	6.9
Background concentrations (ppb)[c]		
[NO]	0.57	0.62
[NO_2]	4.41	4.20
[O_3]	42.25	42.87
[SO_2]	2.10	1.69
[C_2H_6]	7.23	7.23
[C_3H_8]	2.74	2.30
[ALKA]	1.81	1.52
[ETHE]	0.06	0.06
[ALKE]	0.00	0.00
[ISOP]	0.05	0.03
[AROM]	0.06	0.06
[PAN]	0.22	0.23

[a]Calculated from aerosol size distributions reported from Jaenicke [1993]
[b]Assumed [8].
[c]Obtained from USEPA Models-3/CMAQ modeling

APPLICATION OF THE REACTIVE PUFF MODEL TO A POWER PLANT CASE IN KOREA

The previous section demonstrated the simulation capability of the developed reactive puff model. However, the relatively nice agreement presented for the "ocean-case" studies cannot always warrant other applications of the reactive puff model to the land-case study. As discussed earlier, over the land situations, frequent changes in the stability classes and complex terrain structures could hamper the direct applications of the developed reactive puff model to the case studies. In spite of such limitation, we wish to emphasize that the intention of this study is to develop/build a simple and practical reactive puff model with which one can quickly and easily assess the environmental influences of the primary pollutant emissions from newly-built (virtual sources) or already-existing (actual sources) large-scale point sources. Here, as an example case, we applied the developed reactive puff model to a Korean power plant study: Hadong power plant located in a south coastal area of the Korean peninsula. In order to prepare the plume background conditions, the 3D-Eulerian US EPA Model-3/CMAQ v.4.3 simulation results for the spring of 2001 in South Korea were used. The results of the CMAQ model simulations for the spring period are summarized in Table 6. The emission rates of the primary pollutants (NO_x and SO_2) and dominant wind directions were obtained by direct contact with the Hadong power-plant and by using the HYbrid Single Particle Lagrangian Integrated Trajectory (HYSPLIT) model, respectively [16].

The accommodation coefficient (sticking coefficient, α) for heterogeneous reactions in Table 6 was assumed, based on Song et al.'s [8] study, and the aerosol surface areas were also assumed, based on Seinfeld and Pandis [17]. The HYSPLIT analysis results indicated that approximately 83% of the plumes moved toward the ocean

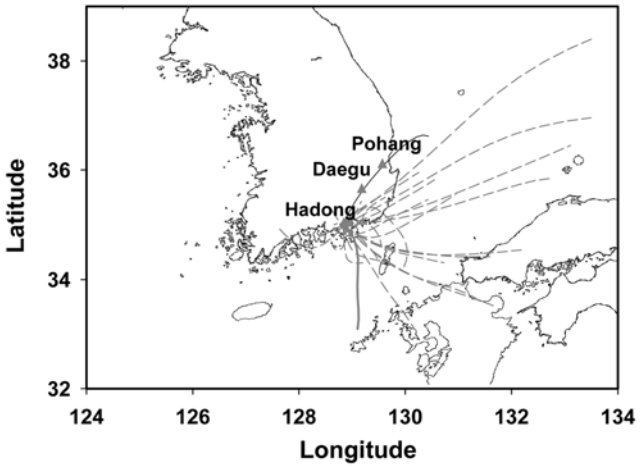

Fig. 6. Forward trajectory analysis of air masses that reached the Hadong power-plant, by using the NOAA HYSPLIT model. Blue and red solid-lines represent the "over-the-land" and "over-the-ocean" case studies.

and the other 17% of the plumes moved to the land areas during the spring season (Fig. 6). To contrast the two types of the plumes, we chose dispersion parameters from the "rural condition over land" (Table 1) and the "ocean case" (Table 2) for the example simulations. In addition, in order to show more vigorous daytime chemistry, the puff from the Hadong power plant was released at 7:00 AM in the morning for the example simulations.

The simulation results are shown in Fig. 7. The panels (a), (c) and (g) of Fig. 7 present the daytime and then nighttime (gray-shading area) concentration profiles of NO_x, O_3, and OH. The concentrations of NO_x, O_3, and OH were a function of the puff travel times (or aging times). The released puffs experienced daytime photochemistry followed by nighttime chemistry. Based on the concentration profiles of NO_x and ozone, the chemical evolution of the plume can be classified as follows: early puff dispersion (stage 1), mid-range dispersion (stage 2), and long-range dispersion (stage 3). Because

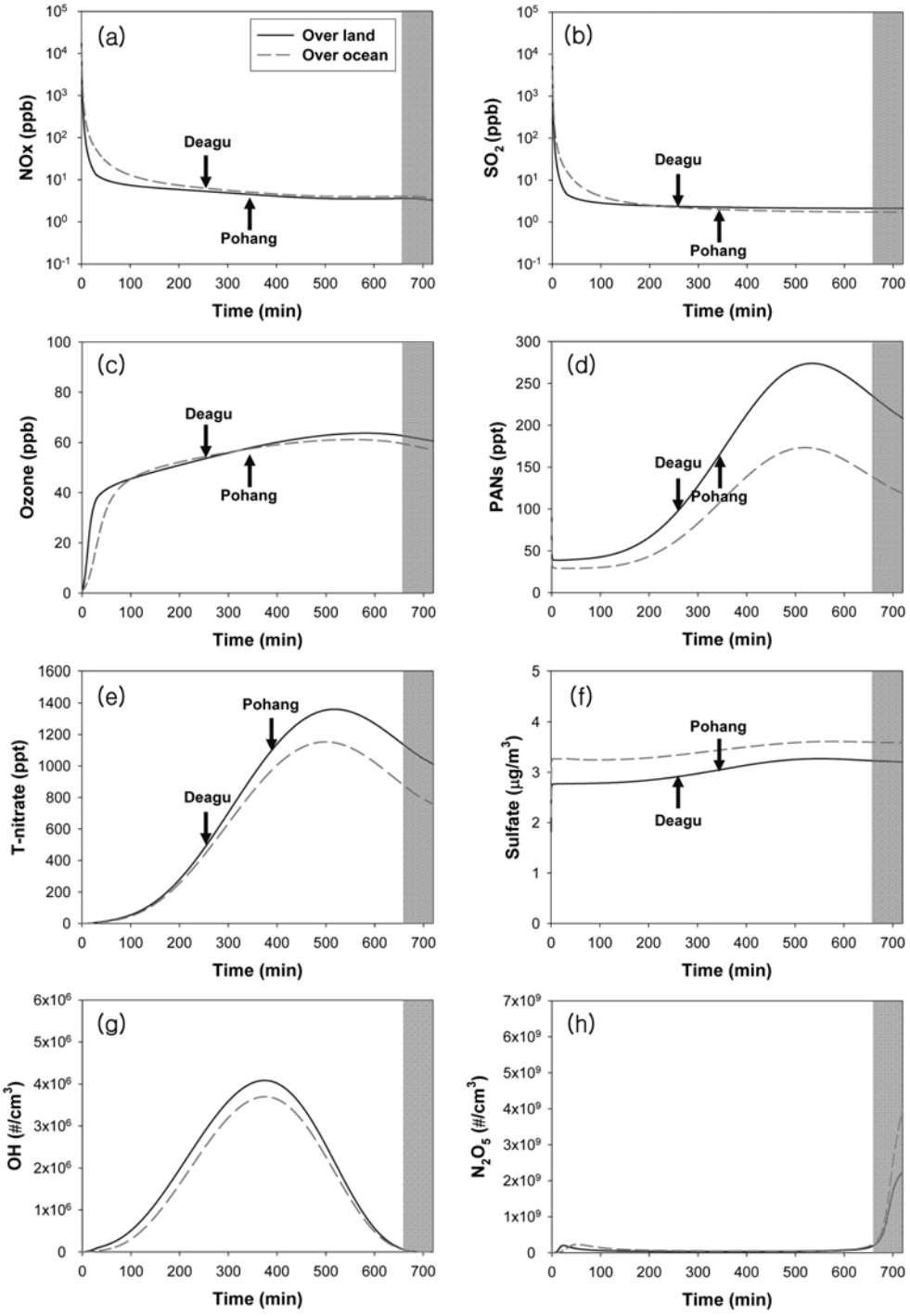

Fig. 7. Puff concentrations of Hadong power-plant plume (the puff was released at 7:00 AM): (a) NO_x, (b) SO_2, (c) Ozone, (d) PANs, (e) T-nitrate, (f) Sulfate, (g) OH, and (h) N_2O_5.

of the high NO concentrations near the power-plant stack, ozone depletion occurred. During stage (1) at which extremely high levels of NO_x were present, NO was oxidized by O_3. The O_3 depletion can clearly be seen in Fig. 7(c). However, as discussed previously, it should be regarded that O_3 during stage (1) was simply stored as the form of NO_2. Due to the depletion process of ozone in the early puff dispersion, OH production was also suppressed by the ozone depletion process (again, refer to [R6] and [R7]). This is shown in panel (g) of Fig. 7, which shows the depleted OH at the early dispersion stage. After the ozone depletion, the concentration of the centerline ozone reached the background ozone level (35.89 ppbv) by two processes: (1) photochemical O_3 production and (2) background O_3 entrainments.

Other secondary toxic pollutants such as T-nitrate (total nitrate≡HNO_3+NO_3^-), PANs (PANs≡TPAN+PAN+MPAN+IPAN), and sulfate (≡SO_4^{2-}) were formed by atmospheric reaction, as shown in panels (d), (e), and (f) of Fig. 7, respectively. The concentration of PANs was also controlled by OH radicals. When the formation of OH radicals was suppressed by the O_3 depletion, the formation of PANs was also suppressed by the low OH levels (refer to [R8]).

$$RCHO+OH \rightarrow RCO+H_2O \quad [R8]$$

$$RCO+O_2 \rightarrow RCO_3 \quad [R9]$$

$$RCO_3+NO_2 \rightarrow PANs \quad [R10]$$

$$PANs+M \rightarrow RCO_3+NO_2 \quad [R11]$$

After suppression of OH radical production, PANs concentrations were increased until 4PM (500 min), and then decreased by decreased OH levels.

The T-nitrate represented the sum of HNO_3 and nitrate. These two N(V) species were produced by the oxidation with OH radicals and heterogeneous reactions at the aerosol surface, as shown below:

$$HNO_3(p) \rightarrow NO_3^-(p)+H^+(aq) \quad [R12]$$

$$N_2O_5+H_2O \rightarrow 2NO_3^-+2H^+ \text{ (heterogeneous)} \quad [R13]$$

$$NO_3 \rightarrow NO_3^- \text{ (p) (heterogeneous)} \quad [R14]$$

During the daytime, T-nitrate was again controlled by the oxidation with OH, because the concentrations of N_2O_5 and NO_3 were negligible (both are regarded as nighttime species). The formations of T-nitrate and sulfate were also controlled by the suppression of OH, as mentioned previously (refer to [R4] & [R5]). Here, sulfate (S(VI)) was mainly formed via (i) heterogeneous oxidation of SO_2 (S(VI)) with, H_2O_2 and/or O_3 and (ii) heterogeneous partitioning of H_2SO_4.

The levels of N_2O_5 are also shown in Fig. 7(h). The levels of N_2O_5 increased after sunset (650 min), since it is a nighttime species. Only small amounts of N_2O_5 existed during the daytime. In contrast, OH has a peak concentration at noon, since it is a daytime radical species. Therefore, after sunset the levels of OH radicals decreased.

Collectively, the developed reactive puff model can reasonably well simulate the behavior of the secondary pollutants species inside the power-plant plumes. We have discussed the complex and highly non-linear plume photochemistry with the applications of the developed reactive puff model to the Hadong power plant case. At this point, we again wish to emphasize the main caveats of this study: (1) Concentrations of the primary pollutants, such as NO_x and SO_2, decrease with the plume travel times mainly due to the turbulent plume dispersion. Therefore, their peak concentrations existed near the source area (typically "less populated" area like Hadong); (2) In contrast, the concentrations of highly toxic, secondary air pollutants, such as O_3, PANs, sulfate and nitrate, increase with the plume travel times and then decrease. Because of these non-linear characteristics, their peak concentrations could exist in the highly populated downwind areas. In order to demonstrate the latter, we ran the reactive puff model with "over the land" parameterizations for the Hadong case, the forward trajectory of which is presented by the blue solid-line in Fig. 6. Fig. 7 shows the results of the simulation. The peak concentrations of O_3, PANs, T-nitrate, and sulfate occurred around a highly populated area (around Daegu), as shown in Fig. 7 (a conceptual illustration is also shown in Fig. 8). This fact strongly indicates that when one conducts the EIA for virtual and

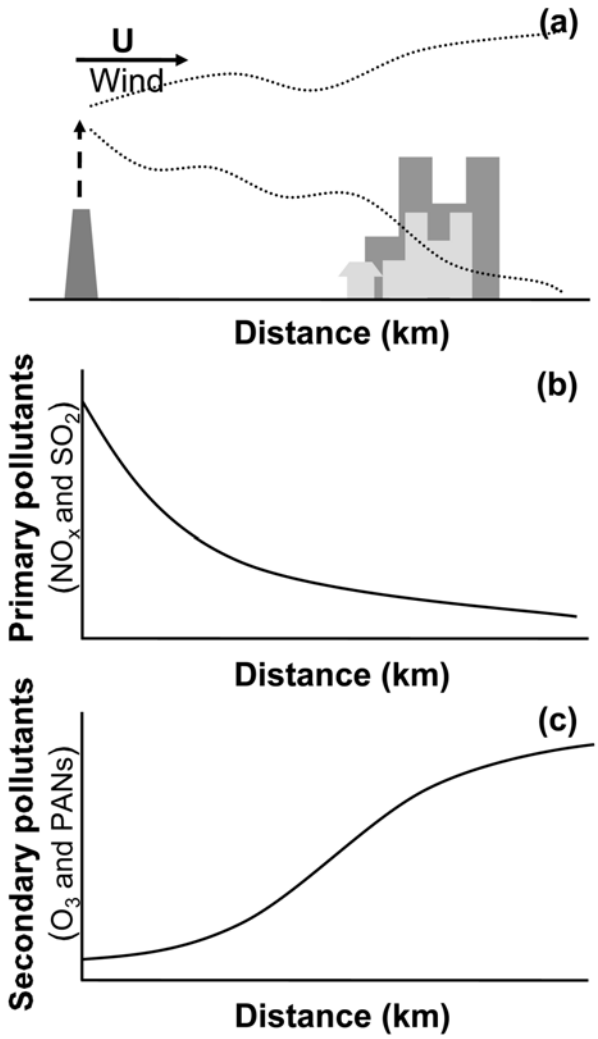

Fig. 8. Pollutant distributions along the puff trajectory: (a) Conceptual illustration of the study case, (b) Distribution of "primary" pollutant concentrations along the puff trajectory, (c) Distribution of "secondary" pollutant concentrations along the puff trajectory.

actual point sources, simply considering the influence of turbulent dispersion of the primary pollutants is not sufficient. In addition, it is absolutely necessary to consider the impacts of the primary pollutants emitted from the large-scale point sources on the formations of the toxic secondary air pollutants downwind the source. For such comprehensive considerations, the reactive puff model was developed in this study.

SUMMARY

This study presented the development of a reactive puff model able to consider turbulent eddy dispersion and chemical transformation simultaneously. Turbulent dispersion was considered by dispersion parameters based on Gaussian plume distribution, while a condensed chemical mechanism based on the modified Lurmann mechanism was incorporated to give considerations for atmospheric chemistry. The results of the model-based predictions were compared with observations obtained from the ITCT 2K2 field campaign data in order to evaluate the performance of the developed plume puff model. The comparison results demonstrated good agreements between the predicted and observed NO_x, SO_2, O_3, and two acid species concentrations. The developed reactive puff model was subsequently applied to a power plant case study in Korea with real emission rates and background conditions obtained from 3-D chemistry-transport modeling over Korea. The case study results revealed the variations of primary and secondary pollutant concentrations due to the chemical and physical components of the model. The developed reactive puff model can be further applied to a more comprehensive EIA, which requires more comprehensive evaluation of the influences of large-scale point sources.

ACKNOWLEDGMENTS

This work was supported by KESRI (R-2005-7-089), which is funded by MOCIE (Ministry of Commerce, Industry and Energy), by the Basic research project through a grant provided by the Gwangju Institute of Science & Technology in 2008, and by Korea Ministry of Environment as an Eco-technopia 21 project under Grant 121-071-055.

REFERENCES

1. Y. S. Ghim and J. Y. Kim, *Korean J. Chem. Eng*., **19**, 52 (2002).
2. EPA, User's guide of the industrial source complex (ISC3) dispersion model (EPA-454/B-95-003a), Environmental Protection Agency, North Carolina 27711.
3. J. S. Scire, D. G. Strimaitis and R. J. Yamartino, A User's Guide for the CALPUFF Dispersion Model (Version 5.0), Earth Tech, Concord, MA (2000).
4. C. A. Briggs, *Atmos. Environ*., **6**, 507 (1972).
5. S. R. Hanna, G. A. Briggs and R. P. Hosker Jr., *Handbook on atmospheric diffusion*, DOE/TIC-11223. Department of Energy, Washington, DC, 102pp (1982).
6. S. R. Hanna, L. L. Schulman, R. J. Paine, J. Pleim and M. Baer, *Journal of the Air Pollution Control Association*, **35**, 1039 (1985).
7. F. W. Lurmann, A. C. Lloyd and R. Atkinson *Journal of Geophysical Research*, **91**, D10, 10905 (1986).
8. C. H. Song, G. Chen and D. D. Davis, *Atmos. Environ.*, **37**, 2663 (2003).
9 G. D. Hess and H. E. Cope, *Atmos. Environ*., **23**, 2857 (1989).
10. N. Kumar and A. G. Russell, *Journal of Geophysical Research*, **101**, 16,737 (1999).
11. R. Atkinson, D. L. Baulch, R. A. Cox, R. F. Hampton Jr., J. A. Kerr, M. J. Rossi and J. Troe, *J. Phys. Chem. Ref. Data*, **26**(2), 215 (1997).
12. W. B. DeMore, S. P. Sander, D. M. Golden, R. R. Hampton, M. J. Kurylo, C. W. Howard, A. R. Ravishankara, C. E. Kolb and M. J. Molina, *JPL Publ*., **97-4** (1997).
13. J. Crawford, D. D. Davis, J. Olson, G. Chen, S. Liu, G. Gregory, J. Barrick, G. Sachse, S. Sandholm, B. Heike, H. Singh and D. Blake, *Journal of Geophysical Research* **104**, 16255 (1999).
14. R. K. Talukdar, M. K. Gilles, F. BattinLeclerc, A. R. Ravishankara, J. M. Fracheboud, J. J. Orlando and G. S. Tyndall, *Geophys. Res. Lett*., **24**, 1091 (1997).
15. G. M. Frick and W. A. Hopel, *J. Atmos. Sci*., **57**, 2625 (2000).
16. R. R. Draxler and G. D. Hess, *Aust. Met. Mag*., **47**, 295 (1998).
17. J. H. Seinfeld and S. N. Pandis, *Atmospheric chemistry and physics*, A Wiley-Interscience, New York, 429-435 (1998).
18. M. W. Malko and J. Troe, *Int. J. Chem. Kinet*., **14**, 399 (1982).
19. J. N. Pitts Jr., E. Sanhueza, R. Atkinson, W. P. L. Carter, A. M. Winer, G. W. Harris and C. N. Plum, *Int. J. Chem. Kinet*., **16**, 919 (1984).